BACKLASH FAULT SUPPRESSION USING LQ OPTIMAL CONTROL BASED RST CONTROLLERS IN WIND TURBINE SYSTEMS USING BOND GRAPHS AND MATLAB/SIMULINK

Mohamed ARAB*, Abederezak LACHOURI*, Mohamed KERIKEB*, Lamine MEHENNAOUI*, Faouzi BOUCHAREB*

*Automatic Laboratory, Electrical Engieneering Departement, Faculty of Technology, 20 August 1955 University of Skikda, Algeria

mohelectron@yahoo.fr, alachouri@yahoo.fr, mohamedkerikeb@yahoo.com, me_lamine@yahoo.fr, bouchareb.faouzi@gmail.com

received 19 June 2020, revised 1 July 2021, accepted 5 July 2021

Abstract: The presence of backlash in wind turbines is a source of limitations as it introduces nonlinearities that reduce their efficiency in speed/torque control which affect the performance of the power quality. Because of production tolerances during rotation, the teeth contact is lost for a small angle; until it is re-established, it produces a backlash phenomenon. The desire to eliminate this phenomenon is often hard to realise due to the nonlinear dynamic behaviour, which arises with the presence of backlash fault in a system. Therefore, the goal of this study is to develop an LQ optimal control structure in a form of an R-S-T controller in order to reduce the disturbing torque transmitted inside the dead zone of a gearbox in the wind turbine system. The actual system is also developed to be used as a demonstration model at lectures or presentations. The efficacy of the proposed control is illustrated via simulations.

Key words: modeling, bond graph, wind turbine, backlash, quadratic linear control, RST controller

1. INTRODUCTION

Generally, the main problem with wind turbine installations is the quality of energy production, which is usually caused by voltage fluctuations measured from the generators. For this purpose, the wind turbines driven by stochastic wind disturbances, gravitational and gyroscopic loads, are perceived as fluctuating power sources (Tomonobu, 2018). Gearbox failure has been the main cause of many reliability defects for modern wind energy sources. The main gearbox elements subject of this failure are, mesh stiffness, bearing stiffness, damping and gear backlash.

Performance of gear transmission is bound to put forward higher requirements. In actual use, about 50% of wind generator fault occurs in the gear transmission system (Zhao et al., 2015). When the gear is at high speed, factors such as stiffness, processing and assembling error are prone to vibration, thus affecting the transmission system accuracy and stability, it even breaks the teeth destroying the machine and causes other major accidents (Zhao et al., 2015). The wind gust could result in unbalanced aerodynamic loads in the rotor, which leads to the non-torque bending moments that are fed into the gearbox. Large driving torques may lead to contact loss of the missing gear teeth. The bending moments applied on the main shaft could cause the loads on gear teeth to change dramatically.

Backlash or clearance exists in any gear system, either by design or due to manufacturing errors or wear. This backlash may induce vibro-impacts, leading to excessive vibration, noise, and dynamic loads (Amir et al., 2014). The clearance between gear pair teeth, or backlash, is considered to be a potential source of vibration in some research papers (Zhenxing et al., 2017; Ragheb and Ragheb, 2010). The influence of clearance occurs mainly in cases when the torque's mean value is near zero or torque reversals are present in the system (Amir et al., 2014).

In the literature, many solutions have been developed to over come backlash faults and reduce the impact on the life of the drivetrain in modern wind turbine systems (Yangshou et al., 2019). Control of systems with backlash is complicated for high-precision requirements and hence generally a mechanical solution with an anti-backlash arrangement is provided, introducing spring-loaded split gear assemblies, precision gear, inertias or other devices for attenuation. All of these solutions are satisfactory, but they aggravate modelling and system analysis which reduce the control accuracy. In this context, the control of systems with backlash has been the subject of study since the 1940s (Marton and Lantos, 2009; Yonezawa et al., 2019). The main analytical tool to describe the backlash has been the describing function technique. To anticipate these phenomena, there exist mechanical and automatic methods (Ruderman et al., 2018). Some control solutions have been proposed, like in Čulina (2011), Odgaard et al. (2013) and Mordian (2014), where they have studied the influence and the partial compensation of simultaneously acting backlash and coulomb friction in an elastic two-mass system with a speed and position controller.

Recker & al and Tao & Kokotovic have worked on the adaptive control of a system with backlash. On this subject, different mathematical models are proposed: Tao & Kokotovic have modelled the inverse backlash model based on a hysteresis cycle (Gang and Kokotović, 1992). Cadiou & M'Sirdi have developed a differentiable model based on the dead zone characteristics (Cardiou and M'Sirdi, 1995). An approximate inverse of the backlash has often been suggested as a backlash remedy, both in a non-adaptive and an adaptive setting. Modern digital controllers have been developed, such as, state space-

based controllers like a linear quadratic regulator (LQR) (Ruderman et al., 2008), a model reference adaptive controller (MRAC) (Guo-Qiang et al., 2013) and an applied heuristic based fuzzy control (Guo-Qiang et al., 2013; Qikun et al., 2019). The study of the impact of gear train backlash on performance of DFIG wind turbine system (Ganesh et al., 2018), partial offline fuzzy model-predictive pitch controller for large-scale wind-turbines model (Mohamed et al., 2020). The robust control is based on fractional- order controllers (et al., 2020). Another technique based on developing an estimator to periodically estimate the size of backlash in the gear of a wind turbine is established. Lagerberg and Egardt (2007) proposed a switched Kalman filter for estimating the backlash size in automobiles. Makosi et. al. (2017) developed an extended Kalman filter for automotive application by estimating the sum of the half shaft torques, the stiffness and damping of the drive shafts, and the size of the driveline backlash.

The purpose of this paper is to describe the characteristics of backlash, to investigate the drawbacks backlash imposes on the dynamics of wind energy conversion systems (WECSs) that contain backlash in a gearbox and to inquire possibilities of how to neutralise the effects of backlash and eliminate electrical pollution. This study was accomplished according this strategy:

– Using the bond graph as a modelling methodology, the dynamics of WECSs that contain backlash in a gearbox, which can be considered as a well tool, adapted for the analysis of these systems, is investigated. This study illustrates the importance of using a simplified bond graph model properly, which accounts for the reduction in simulation time in comparison with the available software package. The model was developed and simulations were obtained using the 20 sim software package environment.
– The linear quadratic (LQ) optimal control structure in the form of an RST controller for gearbox system's backlash vibration suppression in WECSs for an input–output approach of the optimal control is implemented. This structure has two degrees of freedom: the digital filters R and S are designed in order to achieve the desired regulation performances and the digital filter T is designed afterwards in order to achieve the desired tracking performances. In this context, it is considered that the optimisation is achieved by means of a rotational speedtracking loop. The model was developed and simulations have been carried out using MATLAB/Simulink.

This article is organised as follows: let's start with a brief introduction and then a modelling of the wind turbine system with backlash in section 2. In section 3, a bondgraph model of the wind turbine system is proposed, and the section 4 is devoted to depict the LQR-RST controller for the reduction of the backlash phenomenon. The results of the simulation are presented in section 5. At the end, section 6 includes a short conclusion.

2. SYSTEM MODELING

In this section, the dynamic simulation model is described for the proposed wind turbine energy conversion. The block diagram of the integrated overall system is shown in Fig. 1. This system is adopted from Tao et al. (2014). The wind turbine consists of a rotor mounted to a nacelle and a tower with two or more blades mechanically connected to an electric generator. The gearbox in the mechanical assembly transforms slower rotational speeds of the wind turbine to higher rotational speeds on the electric generator. The rotation of the electric generator's shaft generates electricity whose output is maintained by a control system. Afterwards, each sub-model of the wind turbine system is presented and combined to obtain a complete model of the wind turbine.

The subsystem emphasised in this paper is the influence of the backlash fault in the gearbox part in order to reduce their efficiency in speed/torque control, which affects the performance of the power quality. Therefore, a control system of a wind turbine is developed using the LQ-RST algorithm to optimise the wind turbine energy conversion process in the presence of vibrations caused by the backlash fault. Fig. 1 shows the basic components of the controlled system.

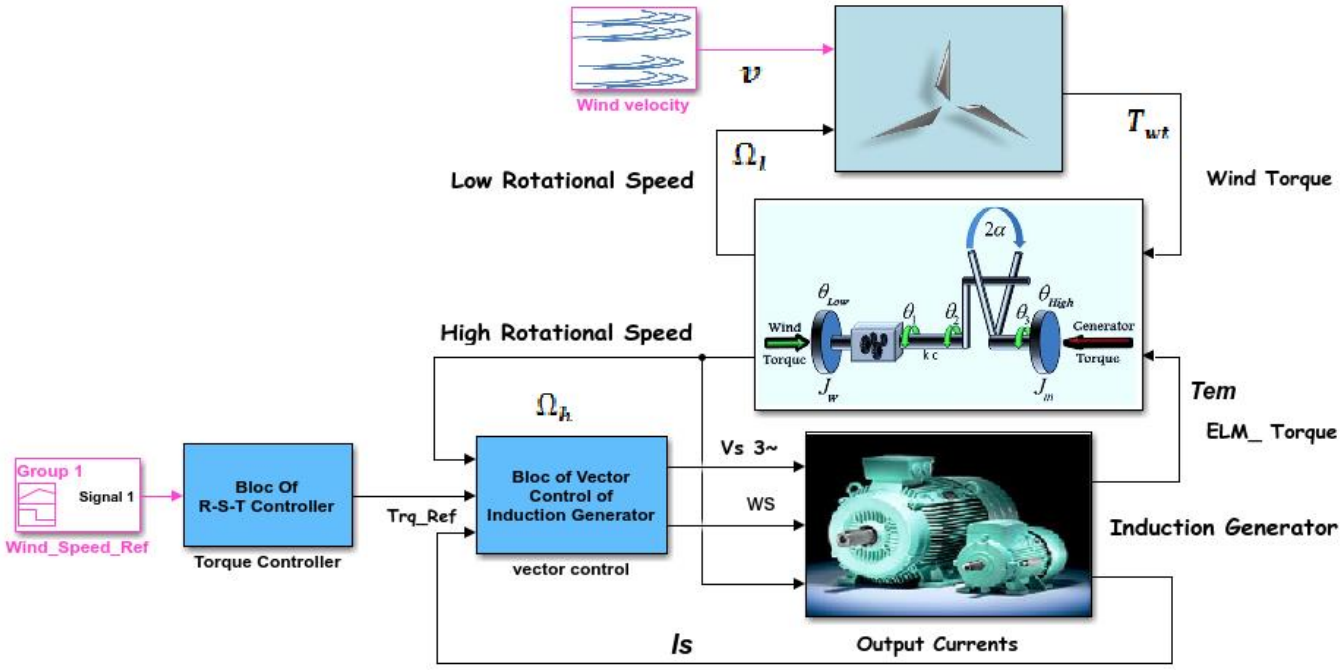

Fig. 1. Block diagram of the controlled wind turbine

2.1. Wind turbine aerodynamic modeling

The aerodynamic part models the extraction of mechanical power from energy in the wind. This part represents the physical rotor blade of the real wind turbine system. The mechanical power is then either fed directly to the electrical part or fed through the mechanical part to the electrical block. The output power of the wind turbine $P_{wt}[w]$ may be calculated from the following equation (Munteanu et al., 2018) :

$$P_{wt} = \frac{1}{2}\rho.\pi.R^2.v^3.C_p(\lambda) \quad (1)$$

In Eq. (1), $\rho[\mathrm{Kg/m^3}]$ is air density, $\mathrm{R[m]}$ is the blade length of a wind turbine, and $\mathrm{C_p}(\lambda)$ is the power coefficient, versus tip speed ratio. The torque developed by the wind turbine may be expressed as follows:

$$T_{wt} = T_{wt}(\Omega_l, v)|_{\beta=constant} \quad (2)$$

where Ω_l is the low-speed shaft rotational speed and β is the pitch angle.

Then, it can be written as follows:

$$T_{wt} = \frac{P_{wt}}{\Omega_l} \quad (3)$$

According to Eq. (1), one obtains the following equation:

$$T_{wt} = \frac{1}{2}\rho.\pi.R^3.v^2.C_T(\lambda) \quad (4)$$

where $C_T = \frac{C_P}{\lambda}$ is the torque coefficient, v is wind speed, $T_{wt}[N.m]$ is wind torque, $T_{em}[N.m]$ is magnetic torque, $\Omega_l[Rad/s]$ is lowspeed, $\Omega_h[Rad/s]$ is highspeed, $\mathrm{T}_{rq\_ref}[N.m]$ is high-speed reference, $I_s[A]$ is stator current, $V_s[V]$ is stator voltage and $w_s[Rad/s]$ is stator frequency.

2.2. Drive train modeling

The mechanical part forms the connection between the aero-dynamic part and the electrical part through torques T_{wt} and T_{em} and speeds Ω_l and Ω_h by the ratio N. The main component of the mechanical part is the gearbox. In this work, we consider coupling speed as a flexible speed; it means that the drive system of the wind turbine will be a three-mass system , as shown in Fig. 2.

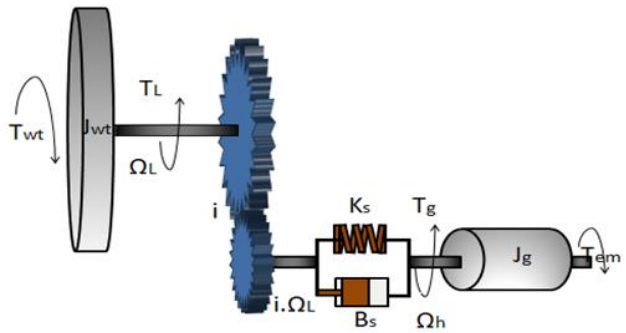

Fig. 2. Three-mass model of a wind turbine drive train

The motion equation is then given as follows:

$$T_{em} = J_g\dot{\Omega}_h + T_{int} \quad (5)$$

In Eq. (5), T_{int} and J_g are the internal torque and the high-speed shaft inertia$[kgm^2]$, respectively. With:

$$T_{int} = K_s\theta_d + b_s\Omega_d \quad (6)$$

$$\theta_d = N\theta_l - \theta_h \quad (7)$$

and:

$$\dot{\theta}_d = N\Omega_l - \Omega_h \quad (8)$$

According to Eqs. (5) and (6), one obtains the following:

$$T_{em} = J_g\dot{\Omega}_h + K_s\theta_d + b_s\Omega_d \quad (9)$$

where k_s is the shaft elasticity $[Nm/rad]$, b_s is the inner damping coefficient of the shaft [kgm^2/s] and θ_d represents the difference in the angle of high-speed shaft θ_h and the low-speed shaft θ_l.

$$T_{wt} = J_{wt}\dot{\Omega}_l + NT_{int} \quad (10)$$

where J_{wt} is shaft inertia with low speed.

2.3. Electrical generator modeling

The electrical part based on induction generators represents the components responsible for converting the mechanical power to electrical power that can be fed into the power grid. In WECSs, the generator interacts with the drivetrain; hence, to this set of equations, the high-speed shaft Ω_h motion is usually added in the following form:

$$J_T\frac{d\Omega_h}{d_t} = T_m - T_{em} \quad (11)$$

where T_m is mechanical torque and J_T is the equivalent inertia rendered to the high-speed shaft. The generator model is described as follows (Naik and Gupta, 2017):

$$\begin{cases} v_{ds} = R_s i_{ds} + \frac{d\lambda_{ds}}{dt} - \omega_s\lambda_{qs} \\ v_{qs} = R_s i_{qs} + \frac{d\lambda_{qs}}{dt} - \omega_s\lambda_{ds} \\ v_{dr} = R_r i_{dr} + \frac{d\lambda_{dr}}{dt} - (\omega_s - \omega_r)\lambda_{qr} = 0 \\ v_{qr} = R_r i_{qr} + \frac{d\lambda_{qr}}{dt} + (\omega_s - \omega_r)\lambda_{dr} = 0 \end{cases} \quad (12)$$

where subscripts $'s'$ and $'r'$ refer to the stator and rotor side, respectively, and subscripts $'d'$ and $'q'$ refer to the dq −axis. The stator and rotor flux can be expressed as follows:

$$\begin{cases} \lambda_{ds} = L_s i_{ds} + L_m i_{dr} \\ \lambda_{qs} = L_s i_{qs} + L_m i_{qr} \\ \lambda_{dr} = L_r i_{dr} + L_m i_{ds} \\ \lambda_{qr} = L_r i_{qr} + L_m i_{qs} \end{cases} \quad (13)$$

where T_{em} can be calculated as follows:

$$T_{em} = \lambda_{qs} i_{ds} - \lambda_{ds} i_{qs} \quad (14)$$

2.4. Backlash model

Backlash can be modeled in many ways. Depending on the needed level of accuracy of the model, different choices can be made (Adlene and Abderrazak, 2018). The definition of backlash

relevant for this paper is defined as 'the play between two physical parts which are supposed to move together and there is an amount of space between the parts'. For electromechanical systems, the growth of wear after a long operating period can engender a non-neglected backlash.

The modeling of this part consists of the following backlash model see (Fig. 1) (Figiel, 2019):

$$\dot{\theta}_b = \begin{cases} Max\left(0, \dot{\theta}_d + \frac{k_s}{b_s}(\theta_d - \theta_b)\right), if \;\; \theta_b = -\alpha \\ \dot{\theta}_d + \frac{k_s}{b_s}(\theta_d - \theta_b), \;\; if \mid \&\theta_b \mid < \alpha \\ Min\left(0, \dot{\theta}_d + \frac{k_s}{b_s}(\theta_d - \theta_b)\right), if \;\; \theta_b = \alpha \end{cases} \quad (15)$$

where θ_b represents the backlash angle, $\theta_b \leq |\alpha|$.

2.5. Bondgraph model of the wind turbine system

Bond graph is a graphical approach to modeling in which component energy ports are connected by bonds that specify the transfer of energy between system components. This formalism facilitates the construction of models that represent the dynamics of multi-domain systems.

The bond graph (BG) contains dissipative, accumulative and conversion elements and junctions. The elements are interconnected by bonds, which carry the exchange variables (general flow and effort) and allow an easy visualisation of the physical system topology and power flow. In addition, to use the BG tool for modeling purposes, its causal and structural properties are also used to study some control problems such as observability, controllability and input–output decoupling.

In this research work, we are interested to present the bond graph modeling of the energy conversion chain. Our goal is first to create a direct model (simulation) with wind speed as the input and rotor speed, electromagnetic torque and the power as outputs by maintaining the power coefficient at the optimum value.

2.5.1. Block diagram of the aerodynamic model part

The diagram model of the aerodynamic part in 20sim software is illustrated in Fig. 3. The wind speed can be considered as the averaged incident wind speed on the swept area by the blades.

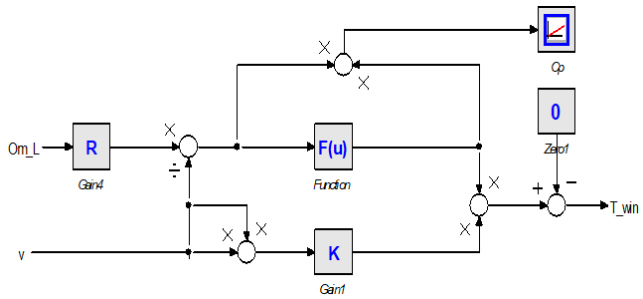

Fig. 3. 20-sim implementation of the aerodynamic model part

2.5.2. Bond-graph model of the drivetrain part

The bond graph implementation of the drivetrain part is shown in Fig. 4. The bond graph model consists of four 1-junctions and one 0-junction. The 1-junction connected to the rotor inertia describes the rotor rotational speed. Since there are dynamics in between the rotor inertia and the generator inertia, they do not have the same speed: this is the reason for the 0-junction.

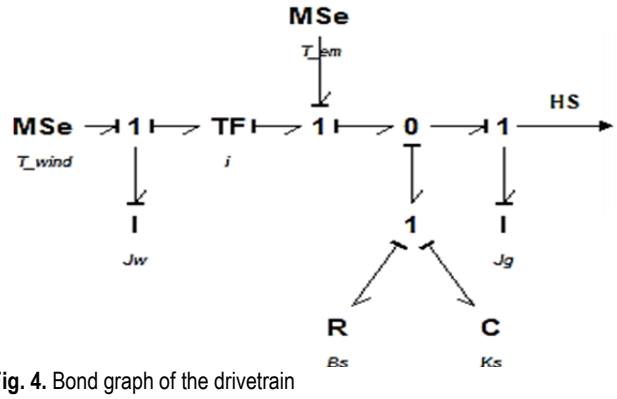

Fig. 4. Bond graph of the drivetrain

2.5.3. Bond Graph model of the electrical part

The bond graph of an induction generator using 20-sim software library is showing in Fig. 5.

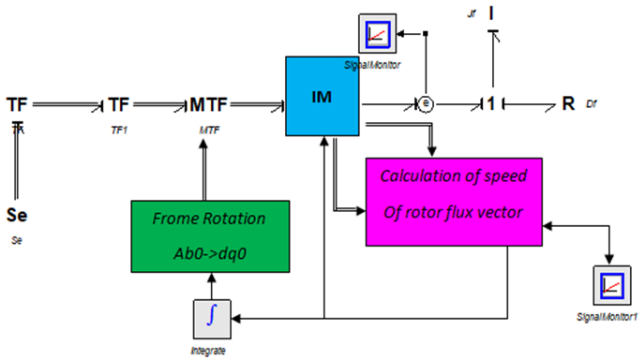

Fig. 5. Induction generator bond graph model

3. CONTROL DESIGN

To illustrate the performance of LQ control in order to eliminate the vibration problem caused by the backlash phenomenon in the wind turbine system, an LQ optimal control structure in the form of an RS controller based on the input–output approach is proposed. As mentioned in introduction, the optimisation is achieved by means of a rotational speed tracking loop based on the minimisation of the tip speed error, $\lambda_{opt} - \lambda(t)$.

3.1. Linear quadratic control of LQ formulation

The LQ control is based on the minimisation of the quadratic criterion which consists in weighting the variances of the control signal $u(k)$ and of $e(k+1)^2$ the tracking error (Mokhtari and Marie, 2012). Let us consider in this study the tracking of a variable rotational speed reference. The identification of the wind turbine system with backlash gave us a transfer function as the following autoregressive–moving-average (ARMA) models form:

$$\text{FTBO} = G(z^{-1}) = \frac{Y(z^{-1})}{U(z^{-1})} = z^{-d} \cdot \frac{B(z^{-1})}{A(z^{-1})} \quad (15)$$

where: $G(z^{-1})$ is the open-loop transfer function with backlash, d is delay time, and $B(z^{-1})$ and $A(z^{-1})$ are the numerator and denominator of the system, respectively, with the following equations:

$$A(z^{-1}) = 1 + a_1 z^{-1} + \dots\dots\dots\dots a_{na} z^{-na} \quad (16)$$

$$B'(z^{-1}) = b_1 z^{-1} + \dots\dots\dots\dots\dots b_{nb} z^{-nb} \quad (17)$$

By the Z inverse transformation of Eq. (15), we obtain the following:

$$A(z^{-1}) \cdot y(k) = B(z^{-1}) \cdot u(k) \quad (18)$$

$$y(k) = -a_1 y(k-1) - \cdots - a_{na} y(k-na) + b_1 u(k-1) + \cdots + b_{nb} u(k-nb-d) \quad (19)$$

Eq. (19) can write as follows:

$$y(k) = -\sum_{i=1}^{na} a_i y(k-i) + \sum_{j=1}^{nb} b_j u(k-j-d) \quad (20)$$

where y: is the system output (high speed: Ω_h) and u is the system control (electromagnetic torque: T_{em}), then we can rewrite Eq. (20) as follows:

$$\Omega_{\boldsymbol{h}}(k) = -\sum_{i=1}^{na} a_i \Omega_{\boldsymbol{h}}(k-i) + \sum_{i=1}^{nb} b_j \boldsymbol{T_{em}}(k-i-d) \quad (21)$$

The simplest expression of the performance criterion given in (Mokhtari and Maria, 2012) is written as follows:

$$J = [e(k+1)]^2 + \beta \cdot \Delta u(k)^2 \quad (22)$$

where: J is the performance criterion, $\Delta u(k)$ is the increment of the system control, β is the weighting coefficient and $[e(k+1)]^2$ is the future error.

With $e(k+1) = [y_{ref}(k+1) - y_{pr}(k+1)]$ (23)

Then,

$$J = \left[y_{ref}(k+1) - y_{pr}(k+1)\right]^2 + \beta \cdot \Delta u(k)^2 \quad (24)$$

and $y_{ref}(k+1)$ is the reference speed $(\boldsymbol{y_{opt}})$. $y_{pr}(k+1)$ is the prediction speed.

To calculate $y_{pr}(k+1)$, we give $d = 0$ and we use Eq. (19) as follows:

$$\begin{aligned} y(k) &= -[a_1 y(k-1) + \cdots + a_{na} y(k-na)] + b_1 u(k-1) + \cdots + b_{nb} u(k-nb) \\ &= -(a_1 z^{-1} + \cdots + a_{na} z^{-na}) \cdot y(k) + (b_1 z^{-1} + \dots + b_{nb} z^{-nb}) \cdot u(k) \\ &= [1 - A(z^{-1})] \cdot y(k) + B(z^{-1}) \cdot u(k) \\ &= Z^{-1} A^*(z^{-1}) \cdot y(k) + Z^{-1}[Z^{-1} B^*(z^{-1}) \cdot y(k) + b_1].u(k) \\ &= A^*(z^{-1}) \cdot y(k-1) + B^*(z^{-1}) \cdot u(k-2) + b_1 \cdot u(k-1) \end{aligned} \quad (25)$$

with

$$A^*(z^{-1}) = -[a_1 + a_2 Z^{-1} + \cdots + a_{na} Z^{-na+1} \quad (26)$$

$$B^*(z^{-1}) = b_2 + a_3 Z^{-1} + \cdots + a_{nb} Z^{-nb+2} \quad (27)$$

To obtain the prediction equation, replace k by k + 1 in the Eq. (25).

$$y_{pr}(k+1) = A^*(z^{-1}) \cdot y(k) + B^*(z^{-1}) \cdot u(k-1) + b_1 \cdot u(k) \quad (28)$$

The derivative of Eq. (28) highlights the control variation $\Delta u(k)$, which gives the output predicted as follows:

$$y_{pr}(k+1) = [1 + A^*(z^{-1})] \cdot y(k) - A^*(z^{-1}) \cdot y(k-1) + B^*(z^{-1}) \cdot u(k-1) + b_1 \cdot \Delta u(k) \quad (29)$$

By replacing Eq. (29) in criterion J (24) we obtain the following:

$$J = \left\{y_{ref}(k+1) - [1 + A^*(z^{-1})]y + A^*(z^{-1}) y(k-1) - B^*(z^{-1}) u(k-1) - b_1 \Delta u(k)\right\}^2 + \beta \Delta u(k)^2 \quad (30)$$

To calculate the optimal variation of an order, it is enough to minimise the criterion J via this equation:

$$\frac{\delta(J)}{\delta(\Delta U)} = 0 \quad (31)$$

Then

$$\Delta u(k) = \eta \begin{pmatrix} y_{ref}(k+1) - [1 + A^*(z^{-1})]y(k) + \\ + A^*(z^{-1}) \cdot y(k-1) - B^*(z^{-1}) \Delta u(k-1) \end{pmatrix} \quad (32)$$

where:

$$\eta = \frac{b_1}{b_1^2 + \beta} \quad (33)$$

The control input value $u(k)$ to be applied at the current time is follows:

$$u(k) = u(k-1) + \Delta u(k) \quad (34)$$

3.2. The RST controller

The RST controller block implements a generalised predictive controller using a reference signal tracking polynomial representation. This type of control is based on the synthesis of a digital controller with two degreesoffreedom. We can simplify Eq. (32) to give the LQ optimal control law as an RST controller illustrated in Fig. 6, and the transfer functions are given as follows:

$$R(z^{-1}) = \eta\{1 + a_1 + (a_2 - a_1) z^{-1} + \cdots + (a_{na} - a_{na-1}) z^{-na+1} - a_{na} z^{-na}\} \quad (35)$$

$$S(z^{-1}) = \left[1 + \eta \begin{pmatrix} b_2 z^{-1} + b_3 z^{-2} + \cdots \\ + b_{nb} z^{-nb+1} \end{pmatrix}\right] \cdot (1 - z^{-1}) \quad (36)$$

$$T(z^{-1}) = \eta \quad (37)$$

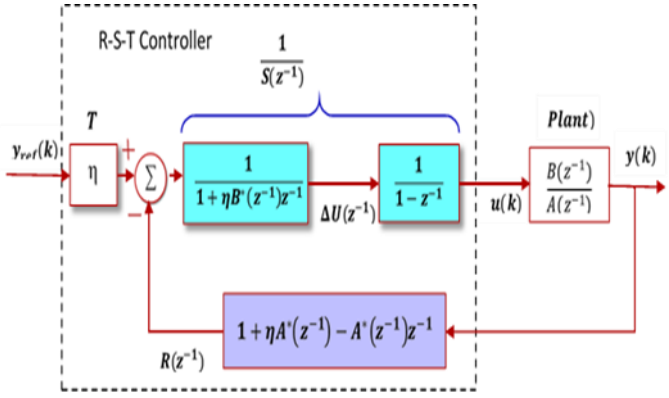

Fig. 6. LQ optimal control structure based on the RST form

DOI 10.2478/ama-2021-0020

4. RESULTS AND SIMULATION

In this section, the adaptive capability and robustness of the proposed LQ-RST algorithm to optimise the wind turbine energy conversion process in the presence of a vibration caused by the backlash fault is demonstrated. The overall model of the wind system was simulated in 20sim software and MATLAB/Simulink/Sim Power Systems environment. The bond graph software 20 sim is object-oriented hierarchical modelling software. It allows users to create models using the bond graph, blockdiagram and equation models. Considering the block diagram illustrated in (Fig. 1), the model includes the wind turbine, induction generator, block of backlash fault and control blocks. The system parameters are presented in Table 1. Several scenarios with changes of backlash magnitude are considered in this study in order to examine the performance of the control system based on the LQ optimal control structure in the form of an RST controller. The asynchronous generator is assumed to have its own speed controller as well as vector controller.

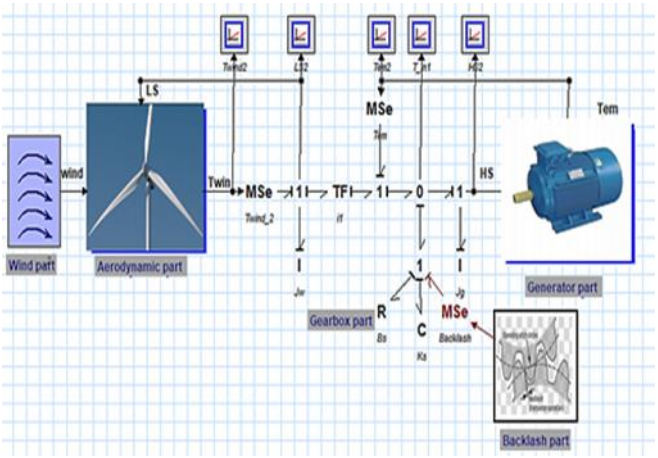

Fig. 7. Bond graph model of the wind turbine system

Tab. 1. Model parameters

Parameter name	Symbol	Value
Frequency	-	50Hz
Nominal power	Pn	6Kw
Multiplier ratio	I	6.25
Air density	P	1.25 kg/m3
Damping coefficient	Bs	2 Kgm^2/s
Number of pairs	P	2
Stator resistance	Rs	1.265 Ω
Rotor resistance	Rr	1.43 mΩ
Stiffness	Ks	75 N/m/Rad
Generator shaft inertia	Jg	0.01 kg/m^2
Inertia of wind turbine	Jwt	3 kg/m^2
Blade length	R	2.5 m
Mutual winding inductance	Lm	0.1397 H
Stator inductance	Ls	0.1452 H
Rotor inductance	Lr	0.1452 H
Max elect-magnetic torque	Tem_max	50 N/m
Stator voltage	Vs	220 V
Stator frequency	ω_s	100 π Rad/s

The following results are obtained by choosing the following values:

✓ R, S and T parameters of the control law are written as follows:

$$\begin{cases} R = -0.1235 + 0.127z^{-1} - 0.05002z^{-2} + 0.004843z^{-3} \\ S = 1 - 1.033z^{-1} + 0.04788z^{-2} - 0.01519z^{-3} \\ T = -0.041755 \end{cases}$$

✓ Backlash magnitude: $\theta_b = 0\ rad, \theta_b = 0.02rad,$ and $\theta_b = 0.04rad$.

In order to assess the proposed control scheme, the simulation was executed according these scenarios:

4.1. Healthy system

This section presents the simulation results without a backlash fault in the wind turbine system. The simulation has been done using a bond graph and MATLAB/Simulink.

Case 01: Step responses for no controlled system

The results of a simulation are obtained with a constant wind velocity having an average speed of 7 m/s. The simulation model based on Fig. 7 presents the bond graph model of the wind turbine system and was constructed in 20-sim software.

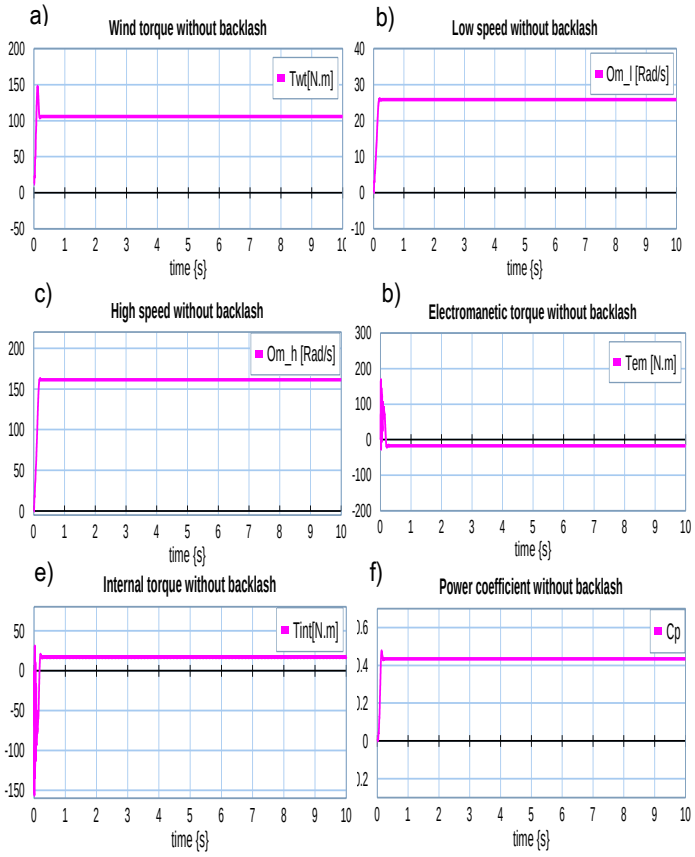

Fig. 8. Healthy system response with no controller (a) wind torque; (b) low speed; (c) high speed; (d) electromagnetic torque; (e) internal torque; (f) power coefficient

Fig. 8 depicts the system responses illustrated in Fig. 7 with zero backlash: (a) wind torque, (b) low speed, (c) high speed, (d) electromagnetic torque, (e) internal torque and (f) power coefficient. With regard to the instantaneous electromagnetic and internal torque (Fig. 8. d, e), we can indicate the presence of oscillations for a very short time at start up. (Fig. 8b and c) show the curve velocities of the multi-mass model. They have strong oscillations in the transient regime during 2s, and it then conversed to its nominal speed at 157rad/s.

Case 02: Responses to the variable profile wind speed for the controlled system

To validate the proposed control system, a wind turbine system based on an induction generator is first tested in ideal conditions and driven to 140 rad/s in MATLAB/Simulink. Different step inputs of rotary speed for reference tracking were applied, and the dynamic responses for the LQ-RST controller are illustrated in Fig. 9.

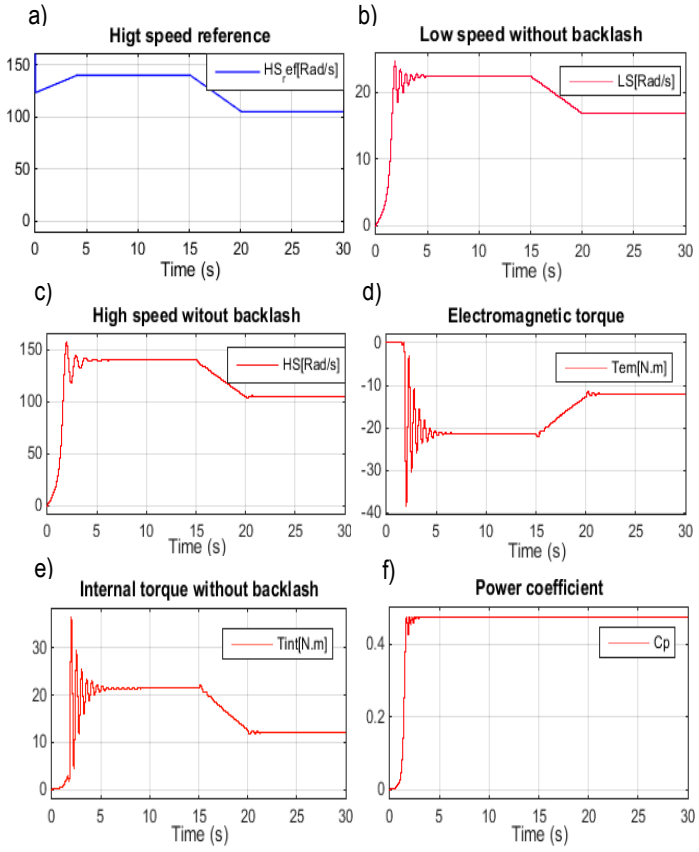

Fig. 9. Healthy system response with a controller. (a) speed reference; (b) low speed; (c) high speed; (d) electromagnetic torque; (e) internal torque; (f) power coefficient

Fig. 9a acts as a reference input for validation purposes and demonstrates the effectiveness of the proposed LQ-RST control algorithm even in the presence of a variable profile wind input. Fig. 9b–f show the performance of the proposed control; all figures show a better performance of the control law; the high velocity follows the reference given by the control and allows us to reduce the torque ripples. The command speed is increased linearly from 0 rad/s to 140 rad/s at $t = 5s$. It is kept constant at 140 rad/s until $t = 15s$, and decreased linearly to 120 rad/s at $t = 20s$. Then, command speed is kept constant at 120 rad/s till $t = 30s$. It can be seen from Fig. 9 b–f that the proposed method of control is able to track quickly the profile of the reference wind velocity. Nevertheless, it shows small oscillations at the time when the variation of the reference wind speed is applied.

4.2. Faulty system

In order to test the performance of the proposed controller (LQ-RST), the value of the backlash magnitude is doubled from 0.02 rad to 0.04 rad with different references tracking. Therefore, the controller should provide good control whatever the variation of the mechanical parameters is.

Case 01: Sinus responses

Fig. 10 a presents a sinusoidal input signal. The response of the system without backlash can be seen in Fig. 10 b. Simulations depicted in Fig. 11 a and b and Fig. 12 a and b illustrate the case with backlash ($\theta_b = 0.02rad$ and $\theta_b = 0.04rad$ respectively). All the waveforms of these figures present oscillations and nonlinearities caused by the backlash phenomenon. In these figures it is well seen that the system with backlash can efficiently affect the power quality.

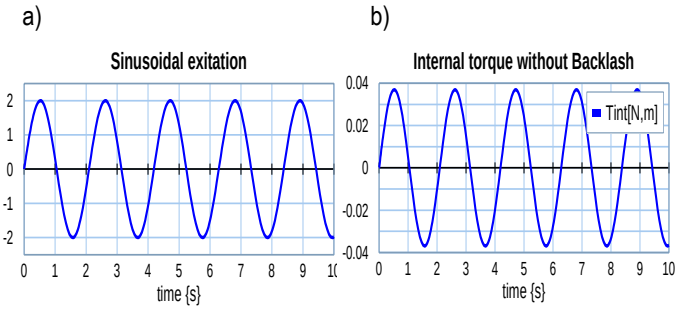

Fig. 10. Healthy response of no controller; **(a)** sinusoidal excitation; **(b)** internal torque

$\boldsymbol{\theta_b = 0.02rad}$: To show the influence of the backlash fault on the system behaviour, we have begun with $\theta_b = 0.02rad$. Fig. 11a and b respectively show the simulated time responses corresponding to backlash angle (θ_b), backlash angular speed ($\dot{\theta}_b$) and internal torque T_{int} (see Eq. (6) and Eq. (15)). It is readily seen from these figures that these estimated variables present a cyclic sudden variation caused by the backlash phenomenon.

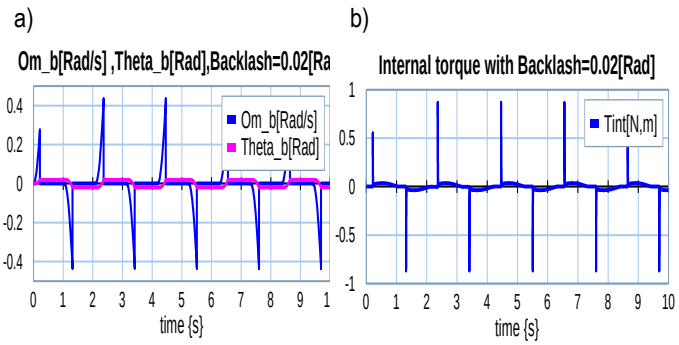

Fig. 11. (a) Backlash angle and backlash position; (b) internal torque

DOI 10.2478/ama-2021-0020

$\boldsymbol{\theta_b = 0.04rad}$**:** However, in order to clearly show this influence, we have to amplify this phenomenon and introduce a fault at level 0.04 rad. Fig. 12a and b show the behavioral response of (θ_b), $(\dot{\theta}_b)$ and internal torque T_{int} and the effect of this phenomenon on the dynamic response of the system. From the figures, we can conclude that the backlash has an important effect and high sensitivity on the mode operating WECSs.

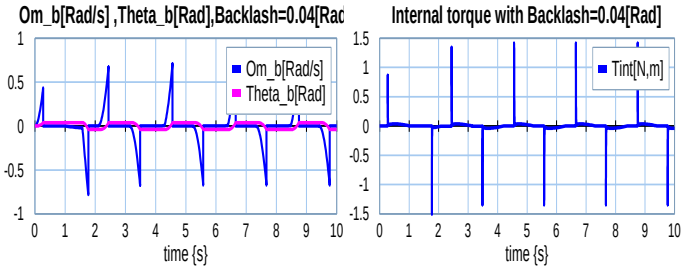

Fig. 12. (a) Backlash angle and backlash position; **(b)** internal torque

Case 02: Responses to the variable profile wind speed for the controlled system

Several scenarios with changes of magnitude of backlash are considered in this study in order to examine the performance of the proposed LQ-RST control algorithm. Measurements were repeated for the case with backlash $(\theta_b = 0.02rad$ and $\theta_b = 0.04rad$ respectively).

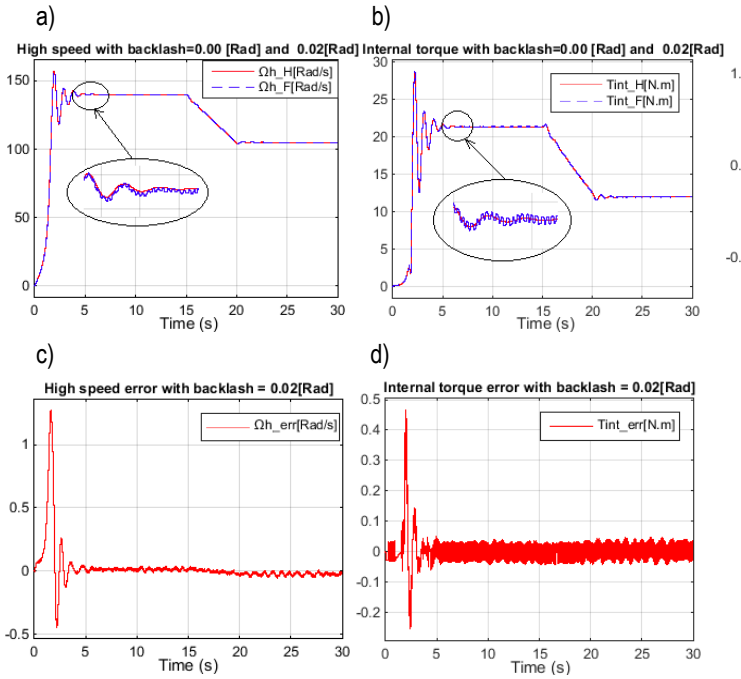

Fig. 13. Faulty system response with a controller: (a) high speed without and with backlash; (b) internal torque without and with backlash; (c) high speed error; (d) internal torque error.

$\boldsymbol{\theta_b = 0.02rad}$ **:** First, robustness tests are made with magnitude of backlash fault at 0.02 rad. The results of these tests are shown in Fig. 13 a and b. By analysing these figures, we can see that the backlash fault does not affect the performance of the operating mode system with a controller scheme. Nevertheless, they show a small oscillation even in the presence of time-varying variations in the profile of wind speed. In addition to this, strategy 'LQ-RST' proves to be the most significant in tracking the system states, for both lower and higher wind speeds, subjected to the variation of the wind speed. Fig. 13 c and d illustrate the residual errors between the healthy and the faulty system response.

$\boldsymbol{\theta_b = 0.04rad}$ **:** Last, robustness tests are made with a dead zone of magnitude at 0.04 rad. Similar results (see Fig. 14 a, b) can be achieved for the LQ-RST controller. These later demonstrate the effectiveness of the proposed control algorithm with evolution of the backlash fault. It is readily seen from Fig. 14 a and b and after zooming around at t =5 s on different responses of the system (such as high speed, low speed, internal torque, etc.) that, we can easily show the oscillation caused by the disturbing torque. Larger variation is augmented and added to the dead zone, Fig. 14 a and b indicate that the LQ-RST controller is limited during this scenario. Fig. 14 c and d) illustrate the residual errors between the healthy and faulty system response.

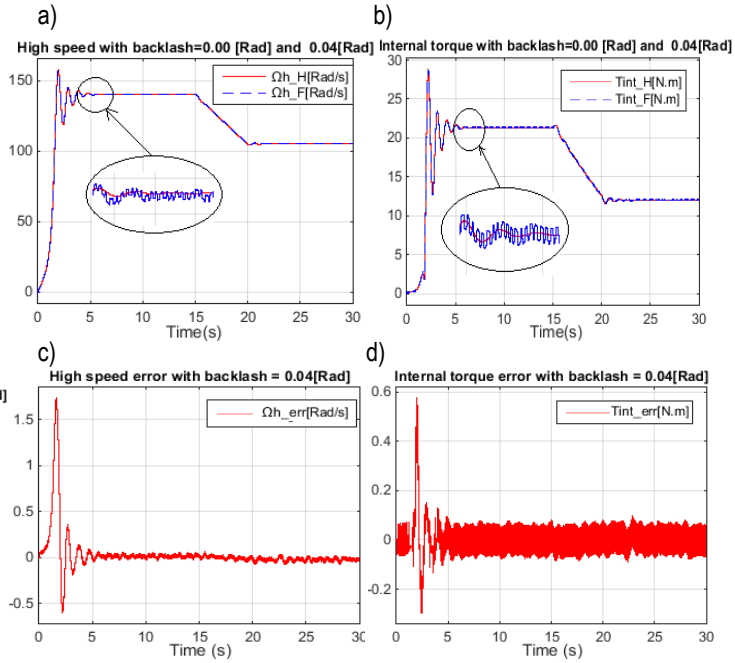

Fig. 14. Faulty system response with a controller; **(a)** high speed without and with backlash; **(b)** internal torque without and with backlash; **(c)** high speed error; **(d)** internal torque error.

Case 03: Responses to sequence wind speed for the controlled system

In this case, we have used a deterministic speed reference covering in steps the operating regimes corresponding to wind speeds from 6 m/s to 11 m/s with the same scenarios of case 2. Similar results (see Figs. 15 a–d, and Fig. 16 a–d) can be achieved for the LQ-RST controller. The efficiency of the LQ-RST controller is proved by means of numerical simulations applied on the wind turbine system with backlash. The LQ-RST Controller for the wind turbine system offers high robustness and fast dynamics. Changing the backlash magnitude approximately from 0.02 rad to 0.04 rad does not affect performance considerably.

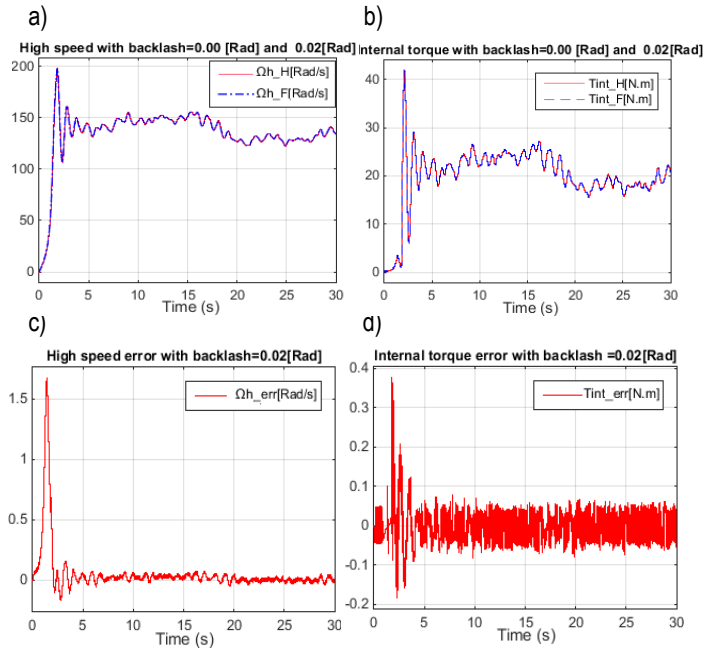

Fig. 15. $\theta_b = 0.02\text{rad}$: Faulty system response with a controller; **(a)** high speed without and with backlash; **(b)** internal torque without and with backlash; **(c)** high speed error; **(d)** internal.

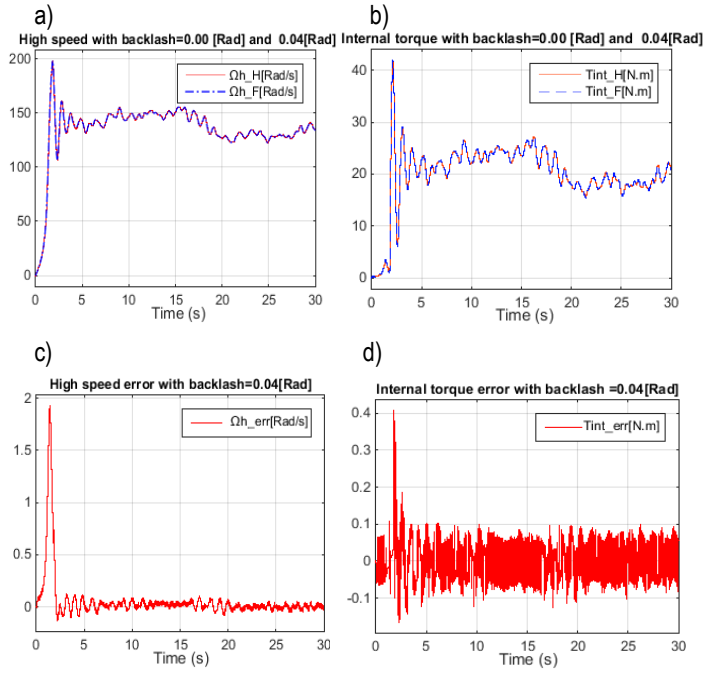

Fig. 16. $\theta_b = 0.04\text{rad}$: Faulty system response with a controller; **(a)** high speed without and with backlash; **(b)** internal torque without and with backlash; **(c)** high speed error; **(d)** internal torque error.

5. CONCLUSION

The purpose of this article was to control the high speed for a WECS with presence of backlash fault in the gearbox part. This is done by first making a BG model for a simplified WECS; the result of this simulation is then compared with that of the model produced with the MATLAB/ Simulink approach. The simulation results of the two approaches are almost the same with small differences, which is why we continued the simulation with MATLAB/Simulink. Many scenarios have been carried out in order to validate the proposed control diagram. The influence of the backlash on the internal torque is clear especially in the excitation by a sinusoidal signal which directly affects the speed of the system and then the quality of energy; this is why we proposed the method of control based on the LQR-RST controller. The work presented demonstrates successful application of the LQR-RST controller to provide robust control under different faulty conditions of the gearbox.

REFERENCES

1. **Adlene R., Abderrazak L.** (2018), Study on the influence of backlash phenomenon on wind turbine power using bond graph approach, *J Braz. Soc. Mech. Sci. Eng.* 40, 91.
2. **Amir R., other authors** (2014), Effects of Floating Sun Gear in a Wind Turbine's Planetary Gearbox with Geometrical Imperfections, *Wind Energy*, 18(12), 2105-2120.
3. **Cadiou J.C., M'Sirdi N.K.** (1995), Modelization and Analysis of a System with Torque Transmitted through a Backlash, *9th world congress on the theory of machines and mechanisms, IFT.MM*, 2, 1467-1470.
4. **Čulina I.** (2011), Desing of mechanical assembly for inversingation of backlash effects in mechatronic systems, *Doctoral dissertation, Fakultet elektrotehnike i računarstva, Sveučilište u Zagrebu*.
5. **Figel K.** (2019), Backlash models for drivability simulation, 10.13140/RG.2.2.29154.79045.
6. **Ganesh P.P., Senroy N., Kar I.N.** (2018), Modeling and impact of gear train backlash on performance of DFIG wind turbine system, *Electric Power Systems Research*, 163, 356–364.
7. **Gang T., Kokotović P.V.** (1992), Adaptive Control of Systems with Backlash, *IFAC Proceedings Volumes*, 25, 87-93.
8. **Guo-Qiang W., Shu-Nan W., Yu-Guang B,. Lei L.** (2013), Experimental studies on model reference adaptive control with integral action employing a rotary encoder and tachometer sensors, *Sensors*, 13(4), 4742–4759.
9. **Lagerberg A., Egardt B.** (2007), Backlash estimation with application to automotive powertrains, *IEEE Transactions on Control Systems Technology*, 15(3), 483–493.
10. **Makosi C.A.M., Rinderknecht S., Binz R., Uphaus F., Kirschbaum F.** (2017), Implementation of an open-loop controller to design the longitudinal vehicle dynamics in passenger cars," *SAE Technical Paper* 2017-01-1107.
11. **Marton L., Lantos B.** (2009), Control of mechanical systems with Stribeck friction and backlash, *Systems and Control Letters*, 58(2), 141-147.
12. **Mohamed A.A., Xiangjie L., Di J.** (2020), Design and implementation of partial offline fuzzy model-predictive pitch controller for large-scale wind-turbines, *Renewable Energy* 145, 981-996.
13. **Mokhtari M., Marie M.** (2012), Engineering Applications of MATLAB® 5.3 and SIMULINK® 3, *Translated from the French by Mohand Mokhtari, Michel Marie, Cécile Davy and Martine Neveu. Springer Science & Business Medi*.
14. **Moradian K.** (2014), Speed control of mechanical systems with backlash, *Indian J. Sci. Res*, 1(2), 94-99.
15. **Munteanu B.A.I., Cutululis N.A., Caenga E.** (2008), Optim. Control Wind Energy Syst. towards a global approach, *Springer Science & Business Media*.
16. **Naik K.A., Gupta C.P.** (2017), Fuzzy logic based pitch angle controller/or SCIG based wind energy system, *In 2017 Recent Developments in Control, Automation & Power Engineering (RDCAPE)* (pp. 60-65), *IEEE*.

17. **Odgaard P.F., Stoustrup J., Kinnaert M.** (2013), Fault-Tolerant Control of Wind Turbines: A Benchmark Model, *IEEE Transactions on Control Systems Technology*, 21(4), 1168-1182.
18. **Qikun S, Yan S, Renfu J, Peng S**. (2019), Design on Type-2 Fuzzy-based Distributed Supervisory Control with Backlash-like Hysteresis, *IEEE Transactions On Fuzzy Systems*, vol, no, pages.
19. **Ragheb A., Ragheb M.** (2010), Wind turbine gearbox technologies, *In Proceedings of the 1st International Nuclear & Renewable Energy Conference (INREC*), 1–8.
20. **Ruderman M,. Yamada S., Fujimoto H.** (2018), Backlash Identification in Two-Mass Systems by Delayed Relay Feedback, Journal of *Dynamic Systems, Measurement, and Control*, 141(6), pages.
21. **Ruderman M., Krettek J., Hoffmann F., Bertram T.** (2008), Optimal state space control of dc motor, *In Proceedings of the 17th world congress the international federation of automatic control. Seoul, Korea*, 5796–5801.
22. **Sami K., other authors** (2020), Maximum power extraction framework using robust fractionalorder feedback linearization control and GM-CPSO for PMSG-based WECS, *Wind Engineering*, vol, no, pages.
23. **Tao L., Zhang B., Feng Z., Zheng B-C.** (2014), Robust Control with Engineering Applications, *Mathematical Problems in Engineering*, vol, no, pages.
24. **Tomonobu S.** (2018), Renewable Energy, *Applied Sciences*, vol, no, pages.
25. **Yangshou X., Kang H., Fengwei X., Yong Y., Meng S., Hua Z.** (2019), Research on the Influence of Backlash on Mesh Stiffness and the Nonlinear Dynamics of Spur Gears, *Applied Sciences*, 9(5), 1029.
26. **Yonezawa H., other authors** (2019), Vibration Control of Automotive Drive System with Nonlinear Gear Backlash, *Journal of Dynamic Systems, Measurement, and Control*, 141(12), pages.
27. **Zhao X., Chen C., Liu J., Zhang L.** (2015), Dynamic Characteristics of a Spur Gear Transmission System for a Wind Turbine. In 2015 International Conference on Automation, *Mechanical Control and Computational Engineering. Atlantis Press*, vol, no, pages.
28. **Zhenxing L., Zhansheng L., Jingming Z., Guanghui Z.** (2017), Study on Interactions Between Tooth Backlash and Journal Bearing Clearance Nonlinearity in Spur Gear Pair System, *Mechanism and Machine Theory*, 107, 229-245.

Mohamed Arab: https://orcid.org/0000-0002-6535-9765
Abederezak Lachouri: https://orcid.org/0000-0001-6718-4228
Mohamed Kerikeb: https://orcid.org/0000-0002-1665-1356
Lamine Mehennaoui: https://orcid.org/0000-0001-6337-6003